CHAPTER-2

ELECTROMAGNETIC CHARACTERIZATION OF A DUST MOLECULAR CLOUD

Abstract: *We study equilibrium electromagnetic properties of a spherically symmetric charged dust molecular cloud (DMC) structure with the help of a new technique based on the modified Lane-Emden equation (m-LEE) of polytropic configuration. First, we methodologically derive the m-LEE under the framework of exact gravito-electrostatic pressure balancing condition. The weak but finite efficacious inertial roles of the thermal species (electrons and ions) on the lowest-order are taken into account. Then, a detailed characterization of the lowest-order Cloud Surface Boundary (CSB) and associated significant parameters on the Jeans scale is numerically obtained and presented. The multi-order extremization of the m-LEE solutions specify the CSB existence at a radial point* 8.58×10^{12} *m relative to the cloud center. It is shown that the CSB gets biased negatively due to the interplay of plasma-boundary wall interaction (global) and plasma sheath-sheath coupling (local) processes. It acts as an interfacial transition layer coupling the bounded and unbounded scale-dynamics of the cloud. The geometrical patterns of the bi-scale plasma coupling are elaborately analyzed. Diversified application of our technique to neutron stars, other observed DMCs and double layers is shown together with future scopes.*

2.1 INTRODUCTION

The dust molecular clouds (DMCs) in the interstellar media are cold, dark, and giant condensed states of the dust and molecular gases giving birth to protostars. The formation of stars and other astrophysical objects within the molecular clouds are complex natural consequences of their low temperatures and high densities, since the gravitational force acting to collapse the cloud may exceed the internal pressures, turbulence, magnetic field and radiation that are acting outward to prevent the collapse. There is observed evidence that the large, star-forming clouds are confined to a large degree by their own gravity (like stars, planets, and galaxies) rather than by external pressures [1-2]. In such self-gravitating clouds, the turbulent velocity field coupled with the thermal instability generates dense structures, some of which are isolated and clumpy, while many

other density structures are contiguous, filament-like. The clumps that satisfy the Jeans criterion, fragment further to form smaller prestellar cores that eventually spawn stars [1-2]. Ambipolar diffusion, the process by which ions drift along magnetic field lines, becomes important in a self-gravitating prestellar core only when it has sufficiently collapsed as to raise its gas temperature whence, molecules rupture to release ions.

As a consequence of gravity-induced electrostatic polarization effect [3-4], large-scale ambipolar non-zero electric field is developed due to gravitational stratification of the ionized constituents, which in turn is responsible for many electromagnetic phenomena sustaining on the new-born stars and their atmospheres like electromagnetic waves, inductive effects, reconnections, and so forth [5-6]. In stellar objects, electromagnetic states, their properties and associated field-induced effects have been discussed by many authors with *Electrical Stellar Models* (ESMs) in past [6-7]. The separation of electrical charge inside a star within the ESM framework has been understood by modelling the star as a ball of hot ionized gas (spherical plasma ball) under the light of basic ionization and diffusion processes. Such dynamic processes allow the stellar structure to acquire a net electrical negative charge $\left(Q_s \sim -10^{10}\, C\right)$ on the surface [6]. Later, however, it has been hypothesized that all gravitationally bounded structures possess net positive charge; whereas, in contrast, expanding intergalactic medium between clusters acquires compensating negative charge at the cost of the expelled electrons [3]. This implies that, as if all astronomical objects like stars, galaxies and clusters of galaxies consist of positively charged clouds embedded in an intergalactic sea of negative charge. In the relativistic regime, unstable polytropic high-compact stellar objects like neutron stars can have a huge amount of charge $\left(Q_s \sim +10^{20}\, C\right)$ under global force-balancing condition [7]. The origin mechanism and maintenance of the high electric field in such astrophysical situations still remains an open problem to be well understood.

The description of stellar structure in both force- and mass-balanced conditions under temperature-independent configurations is usually made by polytropic model defined by the Lane-Emden equation (LEE) of state [9-10]. There indeed exist various exact solutions for diverse equilibrium configurations describable by the LEE and its various other mathematical constructs [10]. The earlier investigations have ignored the plasma-boundary-wall interaction, gravito-electrostatic coupling processes, and collective electrodynamic response scales of the plasma constituents. A full procedural description of the electromagnetic anatomy of the DMCs has been an unavoidable challenge for last few decades from various astrophysical perspectives. In addition,

the inertial effect of the thermal species on such cloud electrodynamics is still unknown. Therefore, there has been a great need for a long period of time for devising a simple self-consistent technique for investigating the electromagnetic cloud properties of basic interest as a function of collective gravitational weight and electrical charge interaction in presence of active inertial roles of the thermal species. This might systematically be explained on a single potential variable of the cloud, its multi-order derivatives and their extreme behavior. In this chapter, motivated by the importance of basic electromagnetic cloud characterization and its expansion, we propose a simple strategy independent of any polytropic index. The lowest-order inertia-corrected thermal species [11] with all the possible thermal effects, gravito-electrostatic coupling, and plasma-boundary-wall interaction processes are taken into account in a spherically symmetric geometry. We build up a modified LEE (*m*-LEE) scheme (after the self-gravitational Poisson formalism) coupling both the electromagnetic [6] and hydrostatic [9, 12-13] behaviors within an integrated gravito-electrostatic framework [12-13]. The model makes a precise examination whether efficacious inertial contribution of the thermal species affects the existence of the Cloud Surface Boundary (CSB), at least, on the lowest-order, by the balanced gravito-electrostatic interaction, which has earlier been found to be located at a radial point $\xi = 3.50$ on the Jeans scale in like situations [14]. Efforts are put to see also the detailed electromagnetic aspects on the entire cloud scale, taking care of both force balancing (electromagnetic) and charge balancing (electrostatic) in the fluid form governed by continuity equation (hydrostatic). The different multi-order derivative constructs of the *m*-LEE on the normalized electrostatic pressure considering weak but finite thermal inertia are methodologically obtained. Besides, the derivatives are shown to have important roles in full electromagnetic CSB specification and in description of its interfacial microphysical processes. It is seen that this model is justifiably successful in the cloud characterization of electromagnetic interest with a single dependent variable in the form of the electric pressure only. The electrostatic pressure arises due to the electrostatic repulsion among the shielded dust grains and their inhomogeneous distribution [12-13]. The model offers an extension for detailed characterization of neutron stars, other observed DMCs, and double layers in space and astrophysical environments.

2.2 PHYSICAL MODEL

We consider an idealized astrophysical multi-fluid model of an external field-free, quasi-neutral, self-gravitating DMC consisting of the thermal electrons, ions, and the inertial dust grains in a

spherically symmetric geometry approximation in hydroelectrostatic equilibrium on the astrophysical scales of space and time. A bulk differential flow is assumed to pre-exist, which is justifiable due to temperature scaling, $T_d << T_e \approx T_i = T$ (for unequal mass scaling, $m_d >> m_i > m_e$; where *T* stands for temperature and *m* for mass of the superscripted species, defined in detail later). Global electrical quasi-neutrality is supposed to subsist over the gravito-electrostatically bounded spherical enclosure containing the plasma volume. The solid matter of the identical spherical dust grains is embedded in the inhomogeneous gaseous phase of the background plasma. We further consider that the heavier grains behave as an inertial fluid, whereas, lighter inertia-corrected electrons and ions as the inertia-modified Boltzmannian thermal particles [11] on the Jeans scale length. So, the grain self-gravitational interaction would be significant even within the Newtonian point-mass approximation [15]. This means that the grain self-gravity would accelerate the cloud contraction against the Coulombic repulsion. This assumption of thermalization is valid provided the phase velocity of intrinsic background fluctuations, if any, is much smaller than their thermal velocity, i.e., any fluctuation in the electron-ion temperature profile is instantly smoothened out. In addition, complications like the effects of dispersed grain rotation, kinetic viscosity, non-thermal energy transport (wave dissipation process) and magnetic field due to involved convective circulation dynamics are neglected for simplification. Such idealization would provide the simplistic equilibrium picture of the cloud and its average behavior, particularly, the CSB in absence of any inductive reconnection process [16].

2.3 MATHEMATICAL ANALYSES

The adopted theoretical model consists of a charged self-gravitating DMC with the thermal electrons, ions and inertial dust grains under hydroelectrostatic equilibrium configuration under spherical symmetry. The light neutral gas particles develop a constant background which is weakly coupled to the collapsing charged grains. The dynamics is described by the continuity, momentum, and the coupling electro-gravitational Poisson equations with all conventional notations. The electron and ion dynamics in unnormalized form are described by,

$$\frac{\partial n_s}{\partial t} + \nabla.\left(n_s \boldsymbol{v}_s\right) = 0 \text{, and} \tag{2.1}$$

$$m_s n_s \left[\frac{\partial \boldsymbol{v}_s}{\partial t} + \left(\boldsymbol{v}_s.\nabla\right)\boldsymbol{v}_s\right] = -q_s n_s \nabla\phi - T_s \nabla n_s \,. \tag{2.2}$$

Here, the label $s = (e, i)$ characterizes the electronic and ionic species with charge $q_e = -e$ and

$q_i = +e$, respectively. Equations (2.1)-(2.2) are respectively the continuity and momentum equations of the flowing electrons and ions with density n_s and velocity v_s.

The massive dust grain dynamics is similarly described by,

$$\frac{\partial n_d}{\partial t} + \nabla.(n_d \boldsymbol{v}_d) = 0, \text{ and} \tag{2.3}$$

$$m_d n_d \left[\frac{\partial \boldsymbol{v}_d}{\partial t} + (\boldsymbol{v}_d.\nabla)\boldsymbol{v}_d \right] = -q_d n_d \nabla\phi - T_d \nabla n_d - m_d n_d \nabla\psi . \tag{2.4}$$

As usual, n_d, and v_d represent number density and velocity of the grains, respectively. The spatial distributions of the electrostatic potential ϕ, and self-gravitational potential ψ in presence of the weak but finite thermal inertia are defined by the closing Poisson equations respectively as follows,

$$\nabla^2\phi = -4\pi\left[e(n_i - n_e) - q_d n_d\right], \text{ and} \tag{2.5}$$

$$\nabla^2\psi = 4\pi G(m_d n_d - m_d n_{do} + m_e n_e + m_i n_i), \tag{2.6}$$

where, $\rho_{d0} = m_d n_{do}$ models the Jeans swindle [5, 17] of the equilibrium unipolar gravitational force field. The swindle provides a formal justification for discarding the unperturbed (zeroth-order) gravitational force field. It allows us to consider the equilibrium initially as 'homogeneous' thereby validating local analysis (as discussed detail in chapter 1). Thus, the full dynamics of the DMC is described by equations (2.1)-(2.6). In gravito-electrostatic equilibrium, the gravitational pressure (P_G) is exactly balanced by the electrostatic pressure (P_E) acting radially in opposite directions ($P_G = -P_E$). Therefore, the DMC equation of force balance [12-13] is given by,

$$\nabla P_E = -\rho_d \nabla\psi . \tag{2.7}$$

Applying equation (2.7), we obtain a conversion relationship between electric charge density (ρ_E) (defined as dust-charge per unit volume), and inertial dust mass density (ρ_d) (defined as dust-mass per unit volume) in gravito-electrostatic equilibrium as,

$$\rho_d = \Gamma\rho_E, \tag{2.8}$$

where, $\Gamma = (4q_d / 3Gm_d)$ is the gravito-electrostatic conversion factor. Here, $\Gamma \approx 1$ for $q_d = 100e$, and $m_d = 3.19\times10^{-7}$ kg [5, 18-20]. So, mass density (ρ_d) is replaced by charge density (ρ_E) in our calculation scheme for a gravito-electrostatically bounded structure characterization. This type of mass-charge density conversion relation has been derived by *Roseeland* under perfect gravito-

electrostatic equilibrium condition [6]. Such conversions have also been adopted in past to see the effect of charged polytropic compact stars in the maximum charge accumulation limit [7]. Applying equations (2.6)-(2.8), we obtain the *m*-LEE for electrostatic pressure (p_E) and charge density (ρ_E) in a spherically symmetric geometry with radial dimension r given as follows,

$$\frac{1}{r^2}\frac{\partial}{\partial r}\left(\frac{r^2}{\rho_E}\frac{\partial p_E}{\partial r}\right) = -4\pi G\rho_E . \tag{2.9}$$

The respective modified normalized Boltzmannian population density distribution of the electrons and ions including their weak but finite inertia are obtained from equations (2.1)-(2.2) with all the usual notations in accordance with the basic rule of inertial drag effects [11], presented as follows,

$$N_e = \exp\left[\left(\frac{1}{2}\right)\frac{m_e}{m_i}M_{eo}^2\left\{1-\exp\left(-2\theta\right)\right\}+\theta\right], \text{ and} \tag{2.10}$$

$$N_i = \exp\left[\left(\frac{1}{2}\right)\frac{m_i}{m_d}M_{io}^2\left\{1-\exp\left(2\theta\right)\right\}-\theta\right]. \tag{2.11}$$

This is worth noticing that equations (2.10)-(2.11) are the lowest-order inertia-corrected population density of the electrons and ions, respectively. If we consider $m_e/m_i, m_i/m_d \to 0$ for the inertialess electrons and ions in equations (2.10)-(2.11), they reduces back to the zero-inertia electrons and ions as given by the normal Boltzmann distribution [12-13].

The electric pressure P_E [12-13] normalized by the equilibrium plasma thermal pressure $P_{E0} = n_0 T$, with inertia-corrected thermal species (equations (2.10)-(2.11)) is derived as,

$$P_E = 2\left[-1-\frac{1}{2}\left(\frac{m_i}{m_d}M_{io}^2+\frac{m_e}{m_i}M_{eo}^2\right)\right]\left[\cosh(\theta)-1\right], \tag{2.12}$$

where, $\theta = e\phi/T$ is the electrostatic potential, developed due to the local charge-imbalance resulting from shielded dust-dust repulsive interaction, normalized by the plasma thermal potential $T/e \sim 1\text{V}$, for $T \sim 1\text{eV}$ [5, 18-20]. Also, N_e, N_i, and N_d are respectively, the population densities of the electrons, ions, and the dust grains normalized by the equilibrium plasma population density n_0. The electron and ion flow velocities (M_{eo}, and M_{io}) are normalized by the ion acoustic phase speed ($C_S = (T/m_i)^{1/2}$), and dust sound phase speed ($C_{SS} = (T/m_d)^{1/2}$), respectively. The velocity normalization is such that the weak but finite inertial effects against the electrodynamic response of both the plasma thermal species becomes realizable [11].

Now, the charge density ρ_E after inertial correction, normalized by equilibrium charge density $\rho_{E0} = n_0 e \sim 1.60\times10^{-12}$ C m^{-3} (for $n_0 = 10^7$ m^{-3}, and $e \sim 1.6\times10^{-19}$ C), is given as follows,

$$\rho_E = \left[1+\frac{1}{2}\left(\frac{m_i}{m_d}M_{io}^2+\frac{m_e}{m_i}M_{eo}^2\right)\right]\{2\,sinh(\theta)\}+Z_d N_d\,. \tag{2.13}$$

Equation (2.9) in the normalized (with standard astrophysical parameters) form with all the usual notations can be simplified into the following,

$$\frac{\alpha}{\xi^2}\frac{\partial}{\partial\xi}\left[\frac{\xi^2}{\rho_E}\left(\frac{\partial P_E}{\partial\xi}\right)\right]=-\rho_E\,. \tag{2.14}$$

Equation (2.14) represents the local relationship between the normalized electric pressure P_E and normalized electric charge density ρ_E , where, $\alpha = n_o/n_{do} \sim 10^3 - 10^4$ [5, 12-13]. Here, n_{do} is the equilibrium dust population density, and $\xi = r/\lambda_J$ is the radial space coordinate normalized by the Jeans scale-length $\lambda_J\,(=C_{ss}/\omega_J)$. The Jeans scale-length (λ_J) is defined as the critical scale-length above which any astrophysical structure, such as molecular cloud, undergoes a gravitational collapse. Also, $\omega_J = (4\pi G\rho_0)^{1/2}$ is the Jeans frequency, and ρ_0 is the inertia-corrected equilibrium mass density of the cloud. The equation (2.14) may be termed as the electrical analogue of the polytropic *m*-LEE with weak thermal inertia. Now, using equations (2.12)-(2.13) to (2.14), and after multiple differentiation, we obtain *m*-LEE on θ-distribution in the following reduced form,

$$\begin{aligned}&\frac{\partial^4\theta}{\partial\xi^4}+C_0\left(\frac{\partial\theta}{\partial\xi}\right)\left(\frac{\partial^3\theta}{\partial\xi^3}\right)+C_1\left(\frac{\partial^3\theta}{\partial\xi^3}\right)+C_2\left(\frac{\partial\theta}{\partial\xi}\right)^2\left(\frac{\partial^2\theta}{\partial\xi^2}\right)+C_3\left(\frac{\partial^2\theta}{\partial\xi^2}\right)^2+C_4\left(\frac{\partial^2\theta}{\partial\xi^2}\right)+C_5\left(\frac{\partial\theta}{\partial\xi}\right)^4\\&+C_6\left(\frac{\partial\theta}{\partial\xi}\right)^2+C_7\left(\frac{\partial\theta}{\partial\xi}\right)=0,\end{aligned} \tag{2.15}$$

where,

$$C_0(\xi)=\frac{2Z_d N_d\,coth(\theta)}{\left[2W_1\,sinh(\theta)+Z_d N_d\right]}, \tag{2.16}$$

$$C_1(\xi)=\frac{2}{\xi}, \tag{2.17}$$

$$C_2(\xi)=-\frac{5Z_d N_d\left[2W_1\,cos\,ech(\theta)+Z_d N_d\,cos\,ech^2(\theta)+2W_1\,coth(\theta)cosh(\theta)\right]}{\left[2W_1\,sinh(\theta)+Z_d N_d\right]^2}, \tag{2.18}$$

$$C_3(\xi)=\frac{2Z_d N_d\, coth(\theta)}{\left[2W_1\, sinh(\theta)+Z_d N_d\right]}, \tag{2.19}$$

$$C_4(\xi)=\frac{\left[4W_1^2\, cosh(\theta)-Z_d^2 N_d^2\, cosh(\theta)cos\, ech^2(\theta)\right]}{2\alpha W_2}-\frac{4}{\xi^2}, \tag{2.20}$$

$$C_5(\xi)=Z_d N_d\left[2W_1\, sinh(\theta)+Z_d N_d\right]^{-3}\begin{bmatrix} 12W_1^2\, coth(\theta)\left\{1+cosh^2(\theta)\right\}- \\ 8W_1^2\, sinh(\theta)cosh(\theta)-4W_1 Z_d N_d\, cosh(\theta)+ \\ 10W_1 Z_d N_d\, cosh(\theta)cos\, ech^2(\theta) \\ +2W_1 Z_d N_d\, sinh(\theta)coth^3(\theta)+ \\ 2(Z_d N_d)^2\, cosh(\theta)cos\, ech^3(\theta) \end{bmatrix}, \tag{2.21}$$

$$C_6(\xi)=\frac{\left[4W_1^2\, sinh(\theta)-(Z_d N_d)^2\, cos\, ech(\theta)+2(Z_d N_d)^2\, coth^2(\theta)cos\, ech(\theta)\right]}{2\alpha W_2}, \text{ and} \tag{2.22}$$

$$C_7(\xi)=\frac{4}{\xi^3}. \tag{2.23}$$

Equation (2.15) is the electrostatic version of the fourth-order *m*-LEE with inertial role of the thermal species. Both the explicit and implicit functional dependences of the variable *m*-LEE coefficients on the plasma and confining geometry parameters are evident from equations (2.16)-(2.23). As a consequence, initial inputs play a vital role in the dynamical evolution of the *m*-LEE. This may be pertinent to add that, if the assumption of spherical symmetry (for radial degree of freedom only) as applied in the presented analysis is dropped, then a more realistic three-dimensional (3-D) picture would come into play. Then, one has to deal with all the components of the relevant potential parameters in spherical polar coordinates (r,θ,ϕ). The analytical calculations would become very complex due to the nonlinear coupling of multi-order spherical harmonics and polynomials. The *m*-LEE might be of different form with diverse complex coefficients and geometrical effects. However, the assumption of spherically symmetric configuration simplifies equation (2.15) to represent the electrostatic version of the fourth-order radially evolving *m*-LEE in differential form. We are interested in the detailed radial profiles of the relevant electromagnetic parameters on the zeroth-order. Being highly complicated, nonlinear and lengthy form, analytical integration for exact solutions is avoided. Applying the fourth-order Runge-Kutta (RK-IV) method, it is numerically integrated as an initial value problem to see the equilibrium structure of the cloud, its lowest-order CSB, associated electromagnetic properties, and transitional behaviors.

2.4 RESULTS AND DISCUSSIONS

Based on the application of a new technique derived from the polytropic *m*-LEE on the Jeans scales of space and time, a theoretical model is developed for investigating the electromagnetic behavior of a simplified self-gravitating spherically symmetric charged dust cloud in an external field-free inhomogeneous hydroelectrostatic equilibrium configuration. The unique originality is the application of the lowest-order inertial correction (weak, but finite; over the zeroth-order inertia) through the modified Boltzmann distributions of the thermal species in the analytical derivation of the multi-order derivative forms of the *m*-LEE on the normalized electrostatic pressure. Different differentials involved in it typify different electromagnetic significances, thereby characterizing diverse cloud properties. So, in order to understand the full electrodynamic cloud features, the multi-order differential forms are numerically integrated under suitable astrophysical conditions. Before presenting the numerical analyses, different normalization constants are estimated methodologically from the available inputs [5, 12-13, 18-21]. An overview of the normalization scheme along with estimated typical values is tabulated in Table 2.1 as follows.

Table 2.1: Normalization constants with estimated typical values

S. No	Physical property	Normalization constant	Typical value
1	Distance	Jeans length [λ_J]	2.45×10^{12} m
2	Electrostatic potential	Cloud thermal potential [T/e]	1.00 V
3	Electric field	Cloud thermal field [$T/e\lambda_J$]	4.08×10^{-13} V m^{-1}
4	Dielectric constant	Permittivity of free space [$\in_0$]	8.85×10^{-12} F m^{-1}
5	Electric pressure	Thermal pressure [$\in_0 T^2/e^2\lambda_J^2$]	1.47×10^{-36} N m^{-2}
6	Electric charge density	Equilibrium charge density [$n_0 e$]	1.60×10^{-12} C m^{-3}
7	Population densities	Equilibrium density [n_0]	1.00×10^{7} m^{-3}
8	Electric energy	Thermal energy [$\in_0 T^2\lambda_J/e^2$]	2.68×10^{1} J
9	Conventional pressure	Thermal pressure [$n_0 T$]	1.60×10^{-12} N m^{-2}
10	Ion flow velocity	Dust-sound phase speed [$C_{SS}=(T/m_d)^{1/2}$]	7.08×10^{-7} m s^{-1}
11	Electron flow velocity	Ion-acoustic phase speed [$C_S=(T/m_i)^{1/2}$]	9.79×10^{3} m s^{-1}

Now, to get the graphical picture, the multi-order differential form (equation (2.15)) of the *m*-LEE is numerically integrated by using the RK-IV method with judicious plasma parameter values [5, 12-13, 18-21] to yield the profiles as shown in figures 2.1-2.5.

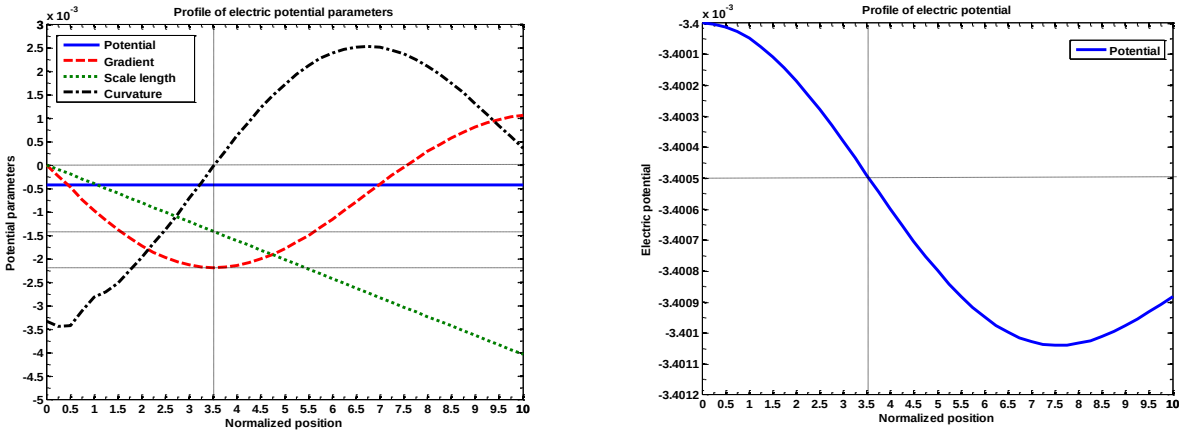

(2.1) **(2.2)**

Figure 2.1 *Profile of the normalized values of (a) electric potential (blue line), (b) potential gradient (red line), (c) potential scale-length (green line), and (d) potential curvature (black line) with normalized position. Various inputs and initial values are given in the text.* ***Figure 2.2*** *Profile of the normalized electric potential with normalized position under the same condition as figure 2.1.*

Figure 2.1 shows the profile of the normalized values of (a) electric potential $\left(\theta = \theta(\xi)\right)$ (rescaled by dividing with 8 and denoted by blue line), (b) potential gradient $\left(\theta_\xi = \partial\theta/\partial\xi\right)$ (rescaled by multiplying with 10^4 and denoted by red line), (c) potential scale-length $\left(L_\theta = \left[\partial(\log\theta)/\partial\xi\right]^{-1}\right)$ (rescaled by multiplying with 3.00×10^{-3} and denoted by green line), and (d) potential curvature $\left(\theta_{\xi\xi} = \partial^2\theta/\partial\xi^2\right)$ (rescaled by multiplying with 3.30×10^6 and denoted by black line) with normalized position. Various numerical input and initial parameter values adopted here are $Z_d = 100$, $N_0 = 1$, $N_d = 2.00\times10^{-3}$, $m_d = 3.19\times10^{-7}$ kg, $\alpha = 5.40\times10^3$, $(\theta)_i = -3.40\times10^{-3}$, $\left(\theta_\xi\right)_i = -1.00\times10^{-10}$, $\left(\theta_{\xi\xi}\right)_i = -1.00\times10^{-7}$, and $\left(\theta_{\xi\xi\xi}\right)_i = 1.00\times10^{-11}$. Figure 2.2 shows the evolutionary profile of the electric potential, specifically as in figure 2.1, but in magnefied form. It is clear that a monotonous potential profile exists in the cloud (Figure 2.2) with a value $\theta \sim -3.4005\times10^{-3}$ ($= -3.4005\times10^{-3}$ V) at $\xi = 3.50$. Beyond this point, nonmonotonous features come into picture. The

lowest-order CSB by the potential gradient minimization (Figure 2.1, red line) is specified to exist at $r = 3.50\lambda_J = 8.58\times10^{12}$ m for $\lambda_J = 2.45\times10^{12}$ m calculated with average interstellar mass density $\sim10^{-28}$ kg m^{-3} [18-20]. The potential scale-length minimization (Figure 2.1, green line), and zero potential-curvature (Figure 2.1, black line) are other characteristic features of the CSB. The value of scale- length at the CSB is $L_{\theta N} \sim -4.67\times10^{-1}$ relative to the center of the cloud. This, physically, is estmated as $L_{\theta Phy} = \lambda_J L_{\theta N} \sim -1.15\times10^{12}$ m. By the terminology 'lowest-order boundary', we mean the nearest spherical electric potential boundary surface (formed by gravito-electrostatic balancing) relative to the center of the self-gravitating cloud mass distribution, such that it behaves as an interfacial transition surface layer exhibiting Bounded Interior Scale (BIS) dynamics on one hand, and Unbounded Exterior Scale (UES) dynamics on the other; as reported earlier in like situations [14]. This is seen that the cloud exhibits perfect quasi-neutrality at the obtained boundary. But, before and after the CSB, an appreciable deviation from quasi-neutrality condition due to gravity-induced polarization is observed (Figure 2.1, black line). These observations are in good agreement with our earlier results on self-gravitating plasma systems with plasma boundary-wall interaction processes taken into account [14]. As one moves away radially outwards relative to that center, the cloud may be found to possess next similar higher-order potential (non-rigid) boundaries, and so forth, as clearly seen from the curvature profiles. Thus, figures 2.1-2.2 show that the CSB is not neutral, but it is electrically charged. Applying the normal Coulomb formula [21], the total electric charge at the CSB is calculated as $Q\,(=4\pi\in_0 r\theta_{Phy}) \sim -3.24\,\mathrm{C}$ for $\theta_{Phy} \sim -3.4005\times10^{-3}$ V. Figure 2.3 displays the profile of the normalized values of (a) electric field $\left(E = -\partial\theta/\partial\xi\right)$ (blue line), (b) field divergence $\left(div\vec{E} = \partial E/\partial\xi\right)$ (red line), (c) field scale-length $\left(L_E = [\partial(log\,E)/\partial\xi]^{-1}\right)$ (rescaled by multiplying with 3.00×10^{-7} and denoted by green line), and (d) field curvature $\left(E_{\xi\xi} = \partial^2 E/\partial\xi^2\right)$ (rescaled by multiplying with 5 and denoted by black line) with normalized position. The field becomes maximum, $E_N = 2.19\times10^{-7}$ with the physical value $E_{Phy}\left(=(T/e\lambda_J)E_N\right) \sim 8.94\times10^{-20}$ V m^{-1} at $\xi = 3.50$, and after that, starts monotonously decresing to a lower value ($\sim -1.01\times10^{-7}$, with physical value $\sim -4.12\times10^{-20}$ V m^{-1}) at $\xi \sim 10.00$ (Figure 2.3, blue line). The field-divergence is zero (Figure 2.3, red line), and the curvature is found to be maximum negative at $\xi = 3.50$ (Figure 2.3, black). Thus, the CSB (on the

lowest-order) by the electric field maximization, vanishing field-divergence, and field curvature minimization is re-specified to exist at $\xi = 3.50$.

We know that for a spherical distribution of electric charge (be it conducting, or nonconducting), the electric field gets maximized only at the surface [22]. So, conversly, if the electric field gets maximized at some radial point relative to some origin, the point corresponds to the location of the nearest (lowest-order) surface boundary relative to the same origin of the considered charge distribution. Therefore, the lowest-order CSB is specifically located at $\xi = 3.50$ based on the electric field maximization principle. This CSB is primarily a field boundary in our model description. Thus, the cloud has no solid physical (rigid) boundary wall, but only a diffuse potential boundary (non-rigid) is found to exist. The cloud electric field itself acts as an electrostatic non-rigid wall having variable strengths against self-gravity enclosing the background plasma volume with the maximum strength at the CSB. The field scale-length at the CSB is $L_{EN} \sim -2.20\times10^{-1}$ (Figure 2.3, green line), which is physically $L_{EPhys} \sim -5.39\times10^{11}$ m. The corresponding strength of the magnetic field at the CSB is semi-empirically estimated as $B_{Phy}(\sim E_{Phy}/c) \sim 2.98\times10^{-28}$ T, where the vacuum light-speed is $c \sim 3\times10^{8}$ m s^{-1} [21]. The magnetic field is too weak to contribute to the cloud dynamics, and hence, neglected at the outset. These findings are found to go in agreement with our earlier results on the self-gravitating plasmas [14]. After the CSB, field reversibility occurs on the unbounded scale at $\xi = 7.75$ due possibly to the surface-charge polarization and interstellar radiation-ionization mechanisms. In the field curvature profile (Figure 2.3, black line), nonmonotonic quasi-neutrality deviation is found to exist at near $\xi = 1$, which is due to the thermal pressure driving wave-instability followed by compression and rarefaction. The deviation is maximum at the CSB with normalized value $E_{\xi\xi N} \sim -4.00\times10^{-8}$, which is physically $E_{\xi\xi Phy} = \left(T/e\lambda_J^3\right)E_{\xi\xi N} \sim -2.72\times10^{-45}$ V m^{-3}. From the CSB on, monotonic deviation results from the random cloud surface-leakage of the electrons and ions due to their high thermal velocities [14]. Figure 2.4 depicts the profile structure of the normalized values of (a) electric pressure $\left(P = 1/2\,\chi E^2\right)$ (blue line), (b) pressure gradient $\left(P_\xi = \partial P/\partial\xi\right)$ (red line), (c) pressure scale-length $\left(L_P = \left[\partial(\log P)/\partial\xi\right]^{-1}\right)$ (rescaled by multiplying with 9.00×10^{-14} and denoted by green line), and (d) pressure curvature $\left(P_{\xi\xi} = \partial^2 P/\partial\xi^2\right)$ (rescaled by multiplying with 2 and denoted by black line) with normalized position. Here, χ is the dielectric constant normalized

by the permittivity of free space, $\in_0 = 8.85\times10^{-12}$ F m^{-1} [21], normally taken in the plasma environment of the DMC, the real value of which is yet to be known. The value of $\chi(=\in/\in_0) \sim 1$, as we consider both the media in the same background. The maximum normalized pressure at the CSB comes out to be $P_N \sim 2.38\times10^{-14}$ (Figure 2.4, blue line), which is physically equal to $P_{Phy} = \left(T^2 \in_0 / e^2\lambda_J^2\right)P_N \sim 3.50\times10^{-50}$ N m^{-2}. The existence of the CSB at $\xi = 3.50$ is further ensured by the joint association of the maximum pressure (Figure 2.4, blue line), zero pressure gradient (Figure 2.4, red line), and minimum pressure curvature (Figure 2.4, black line). The physical value of the pressure curvature at the CSB is $P_{\xi\xi phy} \sim -2.15\times10^{-63}$ N m^{-4} for normalized value $P_{\xi\xi N} \sim -8.75\times10^{-15}$. Their small values are due to the application of the small permittivity value $\in_0$ and application of the inertia-modefied thermal distributions. The normalized value of the scale-length at the CSB is $L_{PN} \sim -1.11\times10^{-1}$, which is physically $L_{PPhy} \sim -2.72\times10^{11}$ m. The electric pressure is maximum at the CSB due to the electrostatic repulsion between shielded dust grains, repulsion between similar thermal species (like polar) and surface-charge polarization. Moreover, as the strength of the electric field decreases outside the CSB, then, the electrostatic pressure also decreases.

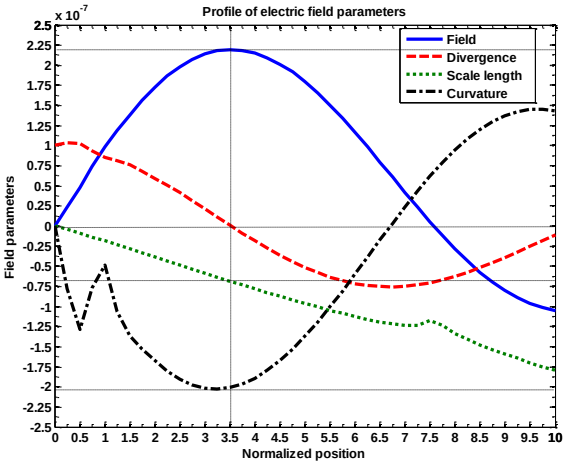

(2.3)

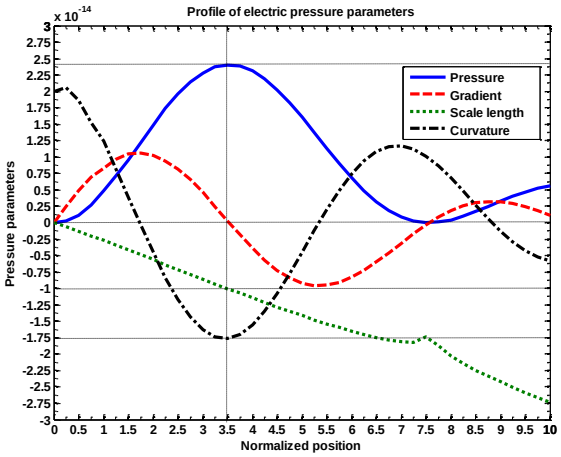

(2.4)

Figure 2.3 *Profile of the normalized values of (a) electric field (blue line), (b) field divergence (red line), (c) field scale-length (green line), and (d) field curvature (black line) with normalized position under same condition as figure 2.1.* ***Figure 2.4*** *Profile of the normalized values of (a) electric pressure (blue line), (b) pressure gradient (red line), (c) pressure scale-length (green line), and (d) pressure curvature (black line) with normalized position under same condition as figure 2.1.*

Figure 2.5 shows the profile of the normalized values of (a) electric energy $\left(U_E = 2/3\pi\chi E^2\xi^3\right)$ (blue line), (b) energy gradient $\left(U_{E\xi} = \partial U/\partial\xi\right)$ (red line), (c) energy scale-length $\left(L_U = [\partial(\log U_E)/\partial\xi]^{-1}\right)$ (rescaled by multiplying with 4.00×10^{-11} and denoted by green line), and (d) energy curvature $\left(U_{E\xi\xi} = \partial^2 U_E/\partial\xi^2\right)$ (black line) with normalized position. The CSB by the zero-energy curvature (Figure 2.5, black line) is further re-specified to lie at $\xi = 3.50$. The energy at the CSB is $U_{EPhy}\left(\left(=\epsilon_0 T^2\lambda_J/e^2\right)U_{EN}\right)\sim 9.48\times10^{-11}$ J for normalized energy $U_{EN}\sim 4.37\times10^{-12}$. The energy shows variable behaviour with maximum strength on the unbounded scale. As already mentioned, in addition to the CSB, there may be higher-order concentric spherical surface boundaries as well. These boundaries are characterized by the extreme behaviours of the relevant physical parameters beyond the CSB. The basic mechanism for such behaviors may be due to the differential flow of the constituents with differential mass-scaling and periodic gravito-acoustic coupling. The scale-length at the CSB is $L_{UN}\sim -1.38\times10^{-1}$, which is physically $L_{UPhy}\sim -3.38\times10^{11}$ m. It is possible to calculate the magnetic energy $U_{MPhy} = 2/3\pi\mu_0 B^2 r^3$ at the CSB. Taking dusty plasma permeability as that of vacuum, $\mu_0 = 4\pi\times10^{-7}$ H m^{-1} [21], the CSB magnetic energy comes out to be $U_{MPhy}\sim 1.47\times10^{-22}$ J. Thus, the physical value of the electrostatic-to-magnetic energy ratio is, $U_{EPhy}/U_{MPhy}\sim 10^{11}$. So, various observed phenomena on the Jeans scale are mainly due to the electrical energy transports only, and not due to the magnetic counterpart. The other electromagnetic properties of the cloud in detail are presented in Ref. [23].

In our model, we neglect various realistic conditions, such as, neutral grain dynamics, the dynamical evolution of background gas, spatiotemporal evolution of the inhomogeneous equilibrium, neutral-charged dust interactions, grain-size, grain-mass distribution, etc. So, we admit that our spherically symmetric model is purely idealized and some deviations may widely exist in reality. Besides, it is developed without the application of any external electromagnetic field, dust-charge fluctuations, etc. All the dissipative agencies are too neglected for simplicity. But, recently, many authors have reported similar results on the relativistic regime for examining the properties of nonlinear field theories embedded in expanding Euclidean Friedmann-Lemaitre-Robertson-Walker metrics in the context of cosmology and the Lagrangian formulation of the stochastic inflationary universe [24]. Their path-integral model approach has shared many

similarities with the quantum Brownian motion and non-equilibrium statistical quantum formalism under dynamical space-time. The model analysis presented here might be extended to the relativistic limit to study the evolutionary patterns of the DMC electromagnetic properties with the spatial expansion of the universe, especially with a mass-hierarchy, as reported before [24].

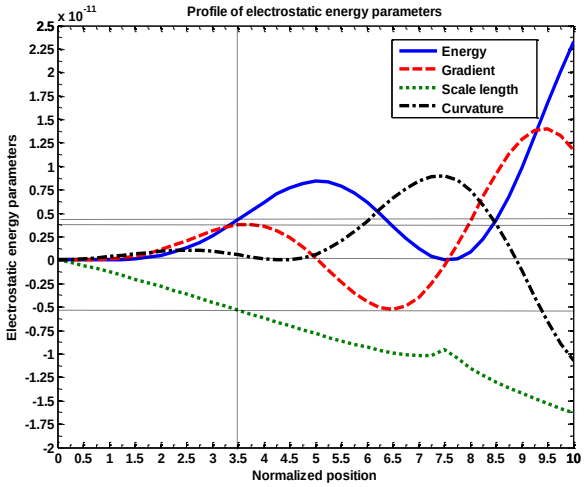

(2.5)

Figure 2.5 *Profile of the normalized values of (a) electric energy (blue line), (b) energy gradient (red line), (c) energy scale-length (green line), and (d) energy curvature (black line) with normalized position under the same condition as figure 2.1.*

It might be relevant to judge the extensive applicability of our model in diverse other astrophysical situations as well. This can be used to extimate different electromagnetic parameters at the surface boundary of neutron star (with surface charge $Q \sim 10^{20} C$) [7], other DMCs such as Barnard 68 (with radius $\sim 1.87\times10^{15}$ m, central population density $\sim 2.00\times10^{11}$ m^{-3}, and dust grain mass $\sim 1.00\times10^{-16}$ kg) [16], 69 and 70 ; Taurus Molecular Cloud 1 (TMC1), Lynds 134N (L134N), and so forth. In addition, the investigation might have astrophysical applications including the Earth's auroral region, extragalactic jets, X-ray and gamma-ray bursts, X-ray pulsars, double radio sources, solar flares, and the source of cosmic ray acceleration like the double layers [8]. One specific example is the double radio galaxy, Cygnus A, with electric field strength $\sim 6.20\times10^{-2}$ V m^{-1} [25], for which the applicability is tested. The estimated values (approximately) of diverse electromagnetic parameters for different astrophysical objects are shown in Table 2.2 as follows.

Table 2.2: Estimated values of electromagnetic parameters

No	Parameter	Astrophysical objects		
		Neutron star	Barnard 68	Cygnus A
1	Charge (Q)	10^{20} C	10^{32} C	5.07×10^{14} C
2	Electric potential (θ_{phy})	1.05×10^{17} V	1.74×10^{29} V	5.32×10^{11} V
3	Potential scale-length ($L_{\theta Phy}$)	8.61×10^{12} m	8.61×10^{12} m	8.61×10^{12} m
4	Electric field (E_{Phy})	1.22×10^{5} V m^{-1}	2.03×10^{16} V m^{-1}	6.20×10^{-2} V m^{-1}
5	Field curvature ($E_{\xi\xi Phy}$)	1.66×10^{-21} V m^{-3}	2.76×10^{-10} V m^{-3}	8.42×10^{-16} V m^{-3}
6	Field scale-length (L_{EPhy})	8.58×10^{12} m	8.58×10^{12} m	8.58×10^{12} m
7	Magnetic field (B_{Phy})	4.07×10^{-5} T	6.77×10^{7} T	2.06×10^{-10} T
8	Electric pressure (P_{Phy})	6.58×10^{-2} N m^{-2}	1.82×10^{21} N m^{-2}	1.70×10^{-14} N m^{-2}
9	Pressure curvature ($P_{\xi\xi Phy}$)	8.94×10^{-28} N m^{-4}	2.47×10^{-5} N m^{-4}	2.30×10^{-40} N m^{-4}
10	Pressure scale-length (L_{PPhy})	8.58×10^{12} m	8.58×10^{12} m	8.58×10^{12} m
11	Electric flux (Φ_{Phy})	1.13×10^{32} V m	1.87×10^{43} V m	5.73×10^{13} V m
12	Flux gradient ($\Phi_{\xi Phy}$)	1.31×10^{19} V	2.17×10^{30} V	6.67 V
13	Flux curvature ($\Phi_{\xi\xi Phy}$)	1.52×10^{6} V m^{-1}	2.52×10^{17} V m^{-1}	7.77×10^{-13} V m^{-1}
14	Flux scale-length ($L_{\Phi Phy}$)	8.58×10^{12} m	8.58×10^{12} m	8.58×10^{12} m
15	Electric energy (U_{EPhy})	2.03×10^{37} J	4.82×10^{60} J	5.08×10^{24} J
16	Energy gradient ($U_{E\xi Phy}$)	2.46×10^{24} J m^{-1}	5.61×10^{47} J m^{-1}	5.92×10^{11} J m^{-1}
17	Energy curvature ($U_{E\xi\xi Phy}$)	2.86×10^{11} J m^{-2}	6.53×10^{24} J m^{-2}	6.89×10^{-2} J m^{-2}
18	Energy scale-length (L_{UPhy})	8.58×10^{12} m	8.58×10^{12} m	8.58×10^{12} m
19	Magnetic energy (U_{MPhy})	3.10×10^{24} J	7.38×10^{48} J	7.07×10^{13} J
20	Electric-to-magnetic energy ratio (U_{EPhy}/U_{MPhy})	10^{11}	10^{11}	10^{11}

2.5 CONCLUSIONS

In this chapter, we study relevant electromagnetic properties of a self-gravitating spherical DMC based on application of the *m*-LEE formalism on the astrophysical space-time scales. The effects of the lowest-order inertial correction of the thermal species are taken into account amid diverse spatial inhomogeneities. The gravito-electrostatic equilibrium structure of the cloud is modeled analytically, graphically and numerically. The basic framework of the *m*-LEE calculation scheme is based on a perfect coupling of the Newtonian and Coulombic dynamics of the fluid cloud constituents. The proposed technique of the cloud characterization lies in the diverse relevant electromagnetic properties, their multi-order gradients, scale-lengths and extreme behaviors on both the bounded and unbounded scales using a single potential variable of electrodynamical significance. In addition, one of the most important conjectures derivable from our investigation is that dust acoustic waves and oscillations are prominent within the interior scale of the plasma volume bounded by the lowest-order CSB (Figures 2.1-2.5) located at $\xi = 3.50$ (on the Jeans scale). This, however, is not so on the unbounded exterior scale and beyond. Thus, it offers a coarse definition and specification of the lowest-order CSB by the principle of extremization of various relevant electromagnetic parameters, and corresponding transitional dynamics. Weaker electromagnetic parameter values at the CSB, and also beyond, are in qualitative conformity with the existing results previously reported in literature [6, 14]. This may equally offer an alternate approach to understand the basic physics of the realistic electromagnetic phenomena occurring in self-gravitating objects like stars, clusters, and their atmospheres through the proposed *m*-LEE framework. This is because this methodological technique conveniently uses a single self-consistent mathematical construct to depict the entire cloud, its non-rigid boundary, transitional behavior, and so forth. Our results are in qualitative agreement as characterized by different space probes, multispace satellite observations, and detectors [15, 26].

Deviating slightly from the principal aim of the study, we examine the applicability of our model for realistic characterization of neutron stars, other observed DMCs, and double layers also together with future expansion possibilities in space and astrophysical environments. It is pertinent to add further that the neutral gas, neutral grains, ions, electrons, and charged grains all need to be considered simultaneously along with suitable equations of state for future refinements. To summarize, we repeat the major conclusive remarks briefly as follows.

(1) The lowest-order CSB demarcating the bounded interior and unbounded exterior scales is precisely determined by a new technique based on the *m*-LEE.

(2) The CSB is found to exist at $\xi = 3.50 = 8.85 \times 10^{12}$ m by the maximization principle of relevant physical parameters.

(3) The radial scale-size of the CSB ($r = \xi\lambda_J = 8.85 \times 10^{12} \sim 10^{13}$ m) is in exact correspondence with that ($L \sim 10^{13}$ m) of the Avinash-Shukla mass limit ($M_{AS} \sim 10^{25}$ kg) with grain-size effect [13].

(4) The physical mechanism responsible for the CSB is the joint action of plasma-wall interaction and plasma sheath-sheath coupling processes.

(5) The basic properties of the DMC are dominated by the electrical parameters as the strength of magnetic field is negligible $\left(U_{EPhy}/U_{MPhy} \sim 10^{11}\right)$, which is in agreement with the reports by others.

(6) Smaller values of various electromagnetic parameters are still debatable for vacuum electric permittivity and magnetic permeability adopted in place of those really unknown for the plasma.

(7) The net charge at the CSB is estimated as $Q \sim -3.24$ C. But, in case of the dust-free gravito-electrostatic sheath model analysis [14], it comes out to be $Q \sim -1.20 \times 10^2$ C. This lowering deviation is due to the loss of the thermal electrons in the charging process of the grains, and the subsequent sheath-sheath interaction developed around each of the shielded grain.

(8) Lastly, we must admit that our model study is a simplified one, originally developed for the DMC characterization with a single key potential parameter only. It is devised under the assumption that the cloud is spherically symmetric, relevant physical parameters have radial components only and it finds an alternate way with the aid of the *m*-LEE instead of going for solving the complicated source equation. In spite of all these idealizations, it may be of extensive applications for further study of the electromagnetic state of diverse astrophysical objects, their constituent dust grains of various characteristics, and ambient dusty atmospheres by an exact polytropic sphere even without any conventional kind of typifying polytropic indices for the degree of astrophysical material concentration towards the center of symmetry.

REFERENCES

1. Gao, Y. and Lou, Yu-Q. Global collapses and expansions in star-forming clouds, *Mon. Not. R. Astron. Soc.* **403**, 1919-1929, 2010.

2. Anathpindika, S. Formation of prestellar cores via non-isothermal gas fragmentation, Pub. Astron. Soc. Australia **32**, 1-21, 2015.
3. Bally, J. and Harrison, E.R. The electrically polarized universe, *Astrophysical Journal* **220**, 743-744, 1978.
4. Vranjes, J. and Tanaka, M. Y. On Gravity Induced Electric Field in Space Plasmas, *Phys. Scr.* **71**, 325-328, 2005.
5. Verheest, F. *Waves in Dusty Space Plasmas*, Kluwer Academic Publishers, Dordrecht, Netherlands, 2000.
6. Rosseland, S. Electrical state of a star, *Mon. Not. Royal Astron. Soc.* **84**, 720-729, 1924.
7. Ray, S., et al. Charged polytropic compact stars, *Braz. J. Phys.* **34**, 310-314, 2004.
8. Alfven, H. Double layers and circuits in astrophysics, *IEEE Trans. Plasma Sci.* **PS-14**, 779-793, 1986.
9. Chandrasekhar, S. *An Introduction to the Study of Stellar Structure*, Dover, New York, 1957.
10. Mirza, B. M. Approximate analytical solutions of the Lane–Emden equation for a self-gravitating isothermal gas sphere, *Mon. Not. R. Astron. Soc.* **395**, 2288-2291, 2009.
11. Deka, U. and Dwivedi, C. B. Effect of electron inertial delay on Debye sheath formation, *Braz. J. Phys.* **40**, 333-339, 2010.
12. Avinash, K. and Shukla, P. K. Gravitational equilibrium and the mass limit for dust clouds, *New J. Phys.* **8**, 1-10, 2006.
13. Avinash, K. Avinash-Shukla mass limit for the maximum dust supported against gravity by electric field, *J. Plasma Phys.* **76**, 493-500, 2010.
14. Dwivedi, C.B., et al. A gravito-electrostatic sheath model for surface origin of subsonic solar wind plasma, *Astrophysical Journal* **663**, 1340-1353, 2007.
15. Kruger, H. and Grun, E. Interstellar dust inside and outside the heliosphere, *Space Sci. Rev.* **143**, 347-356, 2009.
16. Alves, J.F., et al. Internal structure of a cold dark molecular cloud inferred from the extinction of background starlight, *Nature* **409**, 159-161, 2001.
17. Cadez, V. M. Applicability problem of Jeans criterion to a stationary self-gravitating cloud, *Astronomy and Astrophysics* **235**, 242-244, 1990.
18. Spitzer, L., Jr. *Physical Processes in the Interstellar Medium*, WILEY-VCH Verlag GmbH & Co. KGaA, Weinheim, 2004.

19. Mendis, D. A. and Rosenberg, M. Cosmic dusty plasma, *Annu. Rev. Astron. Astrophys.* **32**, 419-463, 1994.
20. Angelis, U. D., et al. Ion plasma waves in dusty plasmas: Halley's comet, *J. Plasma Phys.* **40**, 399-406, 1988.
21. Huba, J. D. *NRL Plasma Formulary*, Naval Research Laboratory, Washington, 2000.
22. Griffiths, D. J. *Introduction to Electrodynamics*, Prentice-Hall of India private limited, New Delhi, 2008.
23. Borah, B. and Karmakar, P. K. A theoretical model for electromagnetic characterization of a spherical dust molecular cloud equilibrium structure, *New Astronomy* **40**, 49-63, 2015.
24. Escudero, C. Nonlinear field theories during homogeneous spatial dilation, *J. Phys. A: Math. Theor.* **46**, 355403(1)- 355403 (9), 2013.
25. Peratt, A. L. Electric space: evolution of the plasma universe, *Astrophys. Space Sci.* **244**, 89-103, 1996.
26. Grun, E., et al. DuneXpress, *Exp. Astron.* **23**, 981-999, 2009.